



# Unveiling the influence of radiation-induced grafting methods on the properties of polyethylene-based anion-exchange membranes for alkaline fuel cells

Ana Laura G. Biancolli<sup>a,\*</sup>, Andrey S. Barbosa<sup>a</sup>, Yasko Kodama<sup>a</sup>, Rogério R. de Sousa Jr.<sup>b</sup>, Alexandre J.C. Lanfredi<sup>b</sup>, Fabio C. Fonseca<sup>a</sup>, José Fernando Q. Rey<sup>b</sup>, Elisabete I. Santiago<sup>a,\*\*</sup>

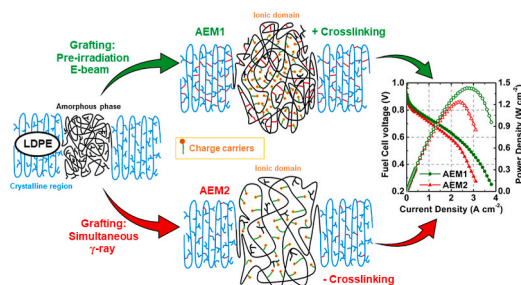
<sup>a</sup> Nuclear and Energy Research Institute, IPEN/CNEN, 05508-000, São Paulo, Brazil

<sup>b</sup> Centre for Engineering, Modelling and Applied Social Sciences, Federal University of ABC UFABC, 09210-580, Santo André, Brazil

## HIGHLIGHTS

- Physicochemical properties of LDPE-AEMs depend on radiation grafting methodology.
- More crosslinking is obtained in LDPE membranes grafted by pre-irradiation method.
- Water absorption is higher for LDPE membranes synthesized by simultaneous grafting method.
- Controlling AEM synthesis parameters can lead to enhanced AEMFC performance.

## GRAPHICAL ABSTRACT



## ARTICLE INFO

### Keywords:

Radiation-induced grafting  
Anion-exchange membrane  
Fuel cell  
Pre-irradiation method  
Simultaneous method  
AEMFC

## ABSTRACT

Anion-exchange membranes (AEM) are envisioned as the enabling materials for the widespread use of cost-effective and efficient polymeric fuel cells. Advancing the understanding of the effect of radiation-induced grafting (RIG) method on the final properties of AEMs is crucial to boost the performance of anion-exchange membrane fuel cells (AEMFCs). The present study provides a systematic investigation of the effect of RIG methods on physicochemical properties of LDPE-based AEMs with similar degree of grafting (DoG) and ion exchange capacity (IEC). Samples grafted by two methods – pre-irradiation (PIM) and simultaneous (SM) – have the same molecular structure, but distinct physicochemical properties due to markedly differences in the degree of crosslinking. Detailed characterization of AEMs showed that RIG method determines the mechanical properties, water transport, and the distribution of ionic groups, which have a direct impact on fuel cell performance and durability. The discussed results show that grafting step directly influences the internal structure and morphology. Controlling the synthesis parameters during RIG is a key feature to design AEMs with enhanced properties that lead to high AEMFC performance and stability.

\* Corresponding author.

\*\* Corresponding author.

E-mail addresses: [anabiancolli@alumni.usp.br](mailto:anabiancolli@alumni.usp.br) (A.L.G. Biancolli), [elisabete.santiago@usp.br](mailto:elisabete.santiago@usp.br) (E.I. Santiago).

## 1. Introduction

Anion-exchange membranes (AEMs) have gained significant attention in the last 10 years due to large applicability in power sources devices, such as fuel cells [1–3] and electrolyzers [4,5], in substitution to proton-exchange membranes (PEMs). The main advantages of AEMs over PEMs in fuel cells are the significantly lower cost compared to state-of-the-art acid membrane (Nafion®), less corrosive environment, and significantly lower crossover of fuels from the anode to the cathode. In the early 2000s, the maximum power densities obtained by anion-exchange membrane fuel cells (AEMFCs) were below 110 mW cm<sup>-2</sup> [1,6]. More recently, reported AEM performances exceeding 1000 mW cm<sup>-2</sup> [7,8] are comparable to the typical values of the well-established proton-exchange membrane fuel cells (PEMFCs). However, despite the remarkable advance in performance, AEMs that reconcile high ionic conductivity with chemical, thermal, and mechanical stabilities are still a challenge for the widespread use of the AEMFCs [3]. In general, the AEMs stability is strongly dependent on the functional groups capable of conducting hydroxide anions [9,10] and the polymer backbone [11,12]. The main cause of AEMs degradation during fuel cell operation is ascribed to the high alkalinity of the medium (hydroxide attacks) [7,13].

Radiation-induced grafting (RIG) has been widely used for the grafting step in AEMs synthesis because of its simplicity and good repeatability [8,14,15]. RIG promotes copolymerization of styrene-based monomers into precursor polymers [16,17], and the subsequent addition of quaternary ammonium-based (QA) functional groups results in the AEMs [10,13,14]. AEMs based on polyethylene (PE), for example, exhibit excellent physicochemical properties, and have proven to be very efficient in energy generation in AEMFCs [8,9,18–20]. Among different PE structures, low-density polyethylene (LDPE) has been employed as a polymeric matrix for AEMs production via RIG because of its high mechanical resistance to radiation and preferential crosslinking pathway due to its high degree of branching [21]. Such crosslinks can significantly enhance the AEM durability properties as a result of backbone reinforcement [18,22].

There are two main methods of obtaining AEMs via RIG: simultaneous (mutual or direct) and pre-irradiation (or indirect) [7,9,23–26]. In the simultaneous method (SM), the polymeric matrix and the monomer are exposed to high-energy radiation, generating free radicals on both reactants that will initiate the monomer copolymerization into the polymeric matrix [9,27]. On the other hand, in the pre-irradiation method (PIM), only the polymer matrix is exposed to ionizing radiation. In this case, grafting step occurs when the pre-irradiated polymer is placed in contact with the non-irradiated monomer. In this method, during irradiation in air, free radicals react with oxygen forming peroxides and hydroperoxides [17,24] which are thermally decomposed to initiate graft polymerization of the monomer in the grafting reaction [28–30].

The preparation of AEMs via RIG depends on the adequate and available radiation source. The use of  $\gamma$ -rays is usually associated with the SM due to the low radiation absorbed dose rates - a fresh source of <sup>60</sup>Co reaches 2.8 10<sup>-3</sup> kGy s<sup>-1</sup>, related to the radioactive source activity [31]. If high dose rates were used for the SM, polymer termination reactions would be more favored, decreasing the chance of reactions between backbone and monomer molecules. In addition, grafting reaction would not be diffusion controlled and it would only take place on the surface of the membrane [17]. Besides, high dose rates result in more homopolymerization, decreasing the monomer availability for grafting reaction [32]. It is possible to find in the literature researches [10,20] using  $\gamma$ -rays for the PIM, however, the degree of grafting (DoG) is usually low, which is not favorable for obtaining AEMs with high ion exchange capacity (IEC). The long time required to reach a certain radiation absorbed dose has been pointed out as the main reason for this feature [31]. In this case, free radicals, which would be available for the grafting reaction later, are recombined in the polymer backbone itself,

undergoing reversible reactions or even oxidative degradation (if irradiated in air atmosphere). Thus, the use of an electron-beam accelerator (EB) is more suitable for the PIM due to its high dose rates [10] (accelerators for research purposes can reach up to 100 kGy s<sup>-1</sup>), which makes it possible to achieve high levels of radiation absorbed dose in a few seconds [31].

Nasef and Hegazy [32] have reported the differences in using both methods in polymer processing. Essentially, the main characteristic of SM is the possibility of using lower absorbed doses than in PIM. Such lower absorbed doses employed in SM methodology can result in higher integrity of the polymeric matrix backbone due to reduced radiation exposure, i.e., lower extent of chain scissions in comparison to PIM. However, the formation of homopolymers is remarkably high due to the concomitant exposure of monomers to ionizing radiation, which can promote a parallel polymerization involving irradiated monomers [17,32]. On the other hand, PIM using EB uses higher adsorbed doses rates and, consequently, shorter time of radiation processing. Also, it enables better control of the post irradiation grafting process by varying the synthesis parameters. An interesting fact is that the increasing availability of EB accelerators compared to  $\gamma$ -rays irradiators makes EB more accessible for large-scale AEMs production [33].

As the high-energy radiation from both the EB accelerators and the  $\gamma$ -rays from <sup>60</sup>Co are much higher than the atomic binding energies, some modifications in the chemical and mechanical properties of synthesized copolymers are expected [27]. Besides the grafting process, parallel reactions, resulting from the combination of radicals in the polymeric backbone, such as crosslinks, end-links, and disproportionation reactions, are usually involved in RIG processes [16,20,34] (see Fig. S1 for main reactions). The ion conduction properties of AEMs, as well as degradation mechanisms, are directly dependent on the modifications resulting from polymer backbone processing [25] and, therefore, on the grafting methodology [10,27].

Despite of several reports on RIG methods, systematic analysis leading to a clear understanding of the effects of the radiation method on the final properties of AEMs for fuel cell applications is missing. In the present study, a systematic analysis of radiation-grafted LDPE-based AEMs produced by simultaneous and pre-irradiation methods provides a detailed correlation between the AEMs' physicochemical properties and electrochemical performance.

## 2. Experimental

### 2.1. AEMs preparation

The synthesis of AEMs followed procedures described in detail elsewhere [7,8,18,35] with few modifications. The radiation-induced grafting step was performed through two methods: i) pre-irradiation (PIM), using an electron-beam accelerator (EB), and ii) simultaneous (SM), using gamma-rays from <sup>60</sup>Co irradiator.

- i) In the pre-irradiation method, LDPE biaxially oriented films (Goodfellow, 25  $\mu$ m) were irradiated in an EB accelerator in air at reduced temperature (film temperature  $\sim -10$  °C was attained by placing it over a layer of dry ice). A Dynamitron Continuous Electron Beam Unit from RDI – Radiation Dynamics Inc. USA, model DC 1500/25/4 - JOB 188 with 1.5 MeV of maximum energy was used. The polymer films were exposed to different radiation absorbed doses: 30, 70, and 100 kGy. The irradiation was performed at 10 kGy per step and higher doses were obtained by sequential steps, with a dose rate of 39.97 kGy s<sup>-1</sup>. The radiation penetration was calculated using the material's density and thickness and the energy used was 0.55 MeV with an EB current of 5.74 mA. The irradiated samples were stored in air atmosphere in a temperature-controlled freezer at  $-40$  °C for a maximum period of 7 days. For the grafting step, the previously irradiated LDPE films were weighed and then immersed in an aqueous solution containing 5% (v/v) of 4-vinylbenzyl chloride (4-

VBC, 90%, Sigma-Aldrich), with previous removal of inhibitors by an Aluminum Oxide (Sigma-Aldrich) column, and 1% (v/v) of surfactant 1-Octyl-2-pyrrolidone (Sigma-Aldrich). The mixture was deoxygenated by purging N<sub>2</sub> for 1 h and then sealed and heated to 55 °C for 5 h.

- ii) In the simultaneous method, the LDPE films and a previously prepared VBC-based monomer solution were placed in 50 mL quartz centrifuge tubes. The solution was prepared by using the method described elsewhere [18] with minor modifications, and consisted of a mixture (v/v) of Tween®20 (Polyethylene glycol sorbitan monolaurate, Sigma-Aldrich), toluene (Neon), 4-VBC (90%, Sigma-Aldrich, without removal of inhibitors) and methanol (Exodo), in the proportion of 1:27:28:44, respectively. The quartz tubes with the solution and the LDPE film were irradiated using a Gammacell 220 type irradiator from Atomic Energy of Canada Ltda. The absorbed doses were 20, 25, and 30 kGy at dose rate of 0.5 kGy h<sup>-1</sup>, thus the reaction times varied from 40 to 60 h.

It is important to mention that due to the dose rate, intrinsic to each technique, it would not be possible to obtain high DoGs using the  $\gamma$ -ray radiation for the PIM. Peroxides and hydroperoxides are very unstable at room temperature and would undergo reversible reactions or oxidative degradation, decreasing the availability of reactive sites for grafting step. Also, it would not be possible to obtain high DoGs using EB for the SM, since the dose rate is extremely high, and the radiation exposure time is very low [32].

For both methods, the VBC-grafted LDPE films were removed from the solution and washed thoroughly with toluene and acetone, followed by drying at room temperature (RT) for 5 h in a vacuum oven.

The amination was carried out by immersing the VBC-grafted LDPE films in aqueous trimethylamine (TMA) solution (~45% vol., Sigma-Aldrich). The samples were kept in TMA solution under stirring for 24 h followed by washing in fresh ultra-pure water (UPW) at 50 °C for 1 h. All membranes were converted to Cl<sup>-</sup> anion by immersion in aqueous NaCl (1 M) overnight with additional two exchanges of solutions every 2 h and then stored in fresh UPW.

Scheme 1 shows the grafting and amination steps involved in the AEMs synthesis. In the PIM (at the top of Scheme 1), LDPE is irradiated in air (step 1) forming peroxides/hydroperoxides which react with the

monomer (step 2) and it is subsequently aminated with TMA in step 3. In the SM (at the bottom of Scheme 1), LDPE film is irradiated with the monomer in step 1, where the grafting occurs concomitantly, and it is aminated with TMA in step 2.

The resulting AEMs are referred according to the grafting method and absorbed dose. For example, 30-EB-PIM refers to the samples irradiated with 30 kGy in the EB accelerator and grafted by the pre-irradiation method. 20- $\gamma$ -SM refers to AEM irradiated with 20 kGy by  $\gamma$ -rays and grafted by the simultaneous method. Grafted-only samples have the prefix “g” and irradiated films (prior to grafting step) have “irrad”, as in the examples: g-20- $\gamma$ -SM and irrad-20- $\gamma$ , respectively.

## 2.2. AEMs characterization

The **degree of grafting** (DoG) of each membrane was calculated according to Equation (1):

$$DoG (\%) = \frac{m_g - m_i}{m_i} \times 100 \quad (1)$$

where “m<sub>g</sub>” is the mass of membrane after grafting and “m<sub>i</sub>” is the initial mass of the irradiated LDPE film.

**Water uptake** (WU) of AEMs in their Cl<sup>-</sup> form was calculated by using Equation (2) [35]. The hydrated mass (m<sub>hyd</sub>) was recorded after soaking AEMs in UPW for 24 h at RT and wiping them in filter paper to eliminate water molecules not trapped inside the samples. The dry mass (m<sub>dry</sub>) was measured after drying samples in a vacuum oven at 50 °C overnight.

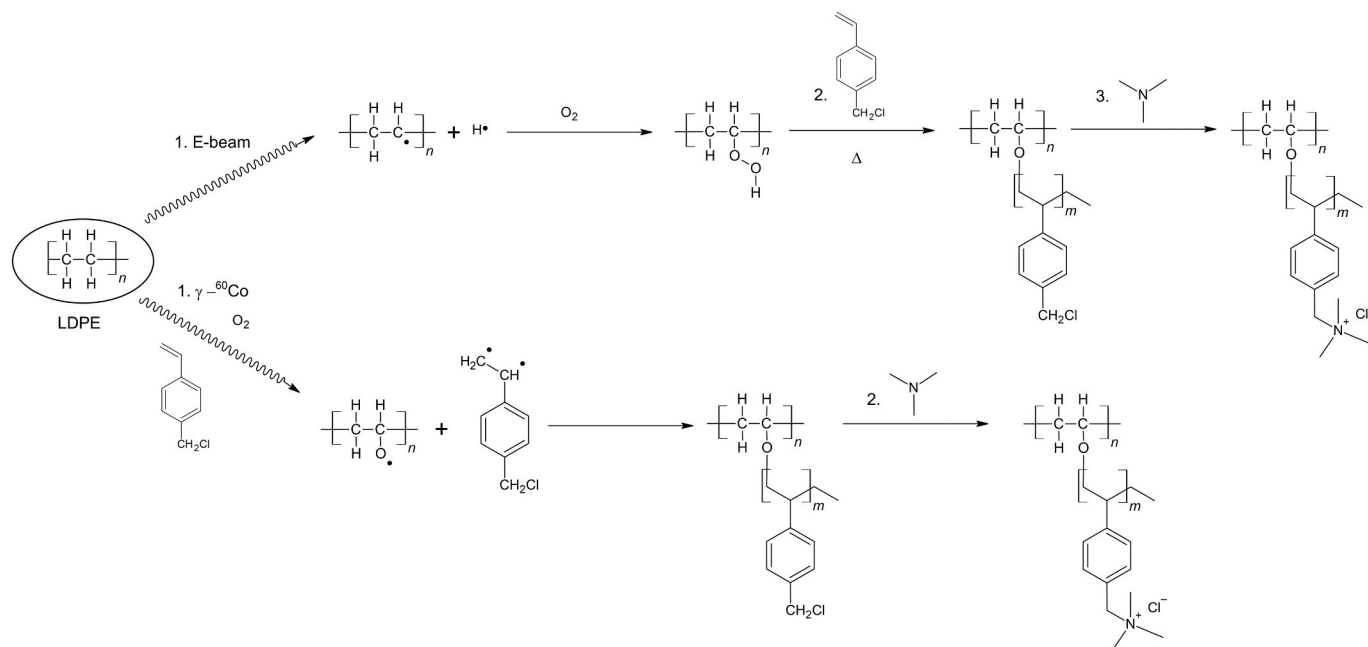
$$WU (\%) = \frac{m_{hyd} - m_{dry}}{m_{dry}} \times 100 \quad (2)$$

The **through-plane swelling** (TPS) – Cl<sup>-</sup> form – was calculated by using Equation (3) [35].

$$TPS (\%) = \frac{t_{hyd} - t_{dry}}{t_{dry}} \times 100 \quad (3)$$

where “t<sub>hyd</sub>” is the thickness of hydrated AEM and “t<sub>dry</sub>” is the thickness of dry AEM.

The **ion exchange capacity** (IEC) of each AEM(Cl<sup>-</sup>) was determined



**Scheme 1.** Representation of reactions involved in the preparation of LDPE-TMA AEMs by the pre-irradiation method (at the top) and the simultaneous method (at the bottom).

by using an automatic titrator (Titrino 848 Plus, Metrohm) equipped with a selective  $\text{Cl}^-$  electrode following a procedure described elsewhere [35].

Finally, the **hydration number** or number of water molecules per anion ( $\lambda$ ) could be calculated according to Equation (4) [36].

$$\lambda = \frac{WU}{IEC (\text{mol g}^{-1}) \cdot M_{\text{H}_2\text{O}} (\text{g mol}^{-1})} \quad (4)$$

### 2.2.1. Raman spectroscopy

A FT-Raman spectrometer (MultiRaman, Bruker Optics) with an excitation laser wavelength source of 1064 nm was used to obtain the Raman spectra of the pristine LDPE, grafted films, and final AEMs( $\text{Cl}^-$ ). The applied laser power was 600 mW and number of scans was 128. The grafting homogeneity through the cross-section of VBC-grafted films was verified by cross-sectional maps recorded using a Raman triple T64000 (Horiba Jobin-Yvon) equipment coupled to a microscope, using a 50 $\times$  objective. Measurements were performed using a laser wavelength of 532 nm, power at sample of 2 mW, and with 5 s of exposure time and 5 accumulations for each spectrum.

### 2.2.2. Gel content (GC)

The gel content (GC) is an indirect method to predict the crosslinking degree of the AEM resultant from the radiation-induced grafted process [37]. Such experiments were conducted aiming at quantifying the insoluble fraction of the polymeric film (gel content). To calculate the GC, LDPE films irradiated by EB (30, 70, and 100 kGy) and  $\gamma$ -rays (20, 25, and 30 kGy) were placed in a Soxhlet extractor, and the extraction followed the ASTM D2765-16 [38] with few adaptations as follows: soluble fraction of LDPE samples was extracted with boiling xylene for 3 h, completing six cycles of extraction. Samples were weighed before (approximately 0.1 g) and after extraction, and the gel content was calculated by using Equation (5) [38]:

$$GC (\%) = \frac{m_f}{m_i} \times 100 \quad (5)$$

where “ $m_f$ ” is the final mass after extraction and “ $m_i$ ” is the initial mass of the film. Samples were vacuum-dried after the extraction and the final weight was recorded when a constant weight was obtained. The GC experiments were done in triplicate.

### 2.2.3. Small-angle X-ray scattering (SAXS)

The SAXS measurements were performed in order to obtain information about the resulting AEM morphology ( $\text{Cl}^-$  form). These experiments were conducted in a Xenocs nano-InXider SAXS equipment, with 938 mm sample to detector distance and 1.541889 Å wavelength. The data was collected at Dectris Pilatus 3 detector with 3660 s exposition time. The data reduction and background subtraction were performed by Chama Xsact 1.8 X-ray Scattering Analysis and Calculation Tool.

### 2.2.4. Tensile tests

The mechanical properties were analyzed by uniaxial tensile testing using a mechanical testing instrument (Instron 5567 model), with a stretching speed of 2 mm  $\text{min}^{-1}$  at RT and ambient conditions.

Rectangular samples (1  $\times$  5  $\text{cm}^2$ ) were dried in a vacuum oven at 50 °C prior to measurements. The dry thickness of each sample can be found in Table 1. A number minimum of 5 specimens of each AEM( $\text{Cl}^-$ ) was tested.

### 2.2.5. Impedance spectroscopy

The ionic conductivity ( $\sigma$ ) of AEMs in  $\text{Cl}^-$  form was measured using a frequency response analyzer (Solartron 1260) in the frequency range of 0.1 Hz–10 MHz with a.c. amplitude of 100 mV. Samples with 1  $\times$  4  $\text{cm}^2$  area were placed in a 4-probe commercial sample holder (FuelCon® TrueXessory-PCM) with an external temperature controller. The conductivity measurements were performed in the 30–90 °C temperature range with full humidification (100% RH). The in-plane conductivity ( $\sigma$ ) was calculated by using Equation (6) [39]

$$\sigma = \frac{d}{R \times w \times t} \quad (6)$$

where “ $d$ ” is the distance between the Pt voltage sense wires (1 cm), “ $R$ ” is the ionic resistance value extracted from the low-frequency X-axis intercepts, “ $w$ ” is the width, and “ $t$ ” is the thickness of the hydrated AEM samples.

The  $\sigma$  of AEM in  $\text{OH}^-$  form was accessed by following the procedure described by Dekel et al. [40,41]. A 1  $\times$  4  $\text{cm}^2$  sample in its  $\text{OH}^-$  form was placed in a 4-probe BT-112 conductivity cell (Scribner Associates), and connected to a Scribner Assoc. 850C fuel cell test station. The measurements were performed between 30 and 90 °C with RH = 100% and a constant  $\text{N}_2$  (99.9992%) flow of 0.5 L  $\text{min}^{-1}$ . A constant voltage was applied during all the experiment to avoid any carbonation in the AEM and to purge out quickly any  $\text{HCO}_3^-$  and  $\text{CO}_3^{2-}$  species, as described by Xinzhi Cao et al. [42], obtaining the called “true  $\text{OH}^-$  conductivity”. The applied voltage was 0.5 V and the current varied from 800 to 1000  $\mu\text{A}$ . Scanning dc sweep from –0.1 V to 0.1 V was performed using an Autolab PGSTAT 302 N each 10 min, 6 times for each cell temperature (after 2 h conditioning at the set temperature). The resistance was obtained by fitting the linear voltage-current data and the conductivity was calculated by using Equation (6) with  $d = 0.425$  cm.

All experiments of this section were done in  $n = 3$  samples of each AEM.

### 2.2.6. Membrane electrode assembly (MEA), fuel cell, and stability tests

The gas diffusion electrode (GDE) method was used for fabricating the AEMFC electrodes. Pt/C (Alfa Aesar, Johnson Matthey HiSpec 4000, 40 wt% Pt) was used as catalyst in the cathodes and PtRu/C (Alfa Aesar, Johnson Matthey HiSpec 12100, 40 wt% Pt and 20 wt% Ru) was used in the anodes. The preparation of the ink followed a procedure described elsewhere [43]. A 2-propanol-based catalytic ink containing 80 wt% of catalyst and 20 wt% of ethylene tetrafluoroethylene (ETFE)-based ionomer [7] was sprayed onto a Toray TGP-H-60 carbon paper gas diffusion substrate (Alfa Aesar, non-teflonated), and then dried in air. The ionomer was prepared by following the procedure in reference [7]. In brief, 5 g of ETFE powder (Fluon® Z-8820X, AGC Europe) were EB irradiated in air with 100 kGy radiation absorbed dose. For grafting reaction, the irradiated powder was immersed in an aqueous solution containing 5%

**Table 1**

Summary of water-related properties of LDPE-based AEMs grafted by PIM and SM and aminated with TMA.

AEM	Grafting and irradiation conditions			WU (%)	$\lambda$	$t_{\text{hyd}}$ ( $\mu\text{m}$ )	$t_{\text{dry}}$ ( $\mu\text{m}$ )	TPS (%)
	Dose (kGy)	Radiation source	Grafting method					
20- $\gamma$ -SM	20	$\gamma$ -rays	SM	69 $\pm$ 2	17	49	45	9
30-EB-PIM	30	EB	PIM	52 $\pm$ 4	13	49	47	4
25- $\gamma$ -SM	25	$\gamma$ -rays	SM	89 $\pm$ 5	20	54	47	15
70-EB-PIM	70	EB	PIM	76 $\pm$ 3	16	57	54	6
30- $\gamma$ -SM	30	$\gamma$ -rays	SM	109 $\pm$ 5	21	60	53	13
100-EB-PIM	100	EB	PIM	95 $\pm$ 4	18	67	61	10

(v/v) of 3,4-VBC (Sigma-Aldrich) and 1% (v/v) of 1-Octyl-2-pyrrolidone (Sigma-Aldrich). The mixture was deoxygenated by purging  $N_2$  for 1 h, then sealed and heated to 60 °C and kept under stirring for 24 h. The grafted-ETFE powders were washed with toluene by filtration and subsequently dried at 50 °C for 5 h in a vacuum oven. For the amination step, grafted ETFE powders were kept under stirring in aqueous trimethylamine (TMA) solution (~45% vol., Sigma-Aldrich) for 24 h, at RT. The ionomer was washed thoroughly with fresh ultra-pure water (UPW) by filtration and then kept in NaCl solution (1 M) overnight, followed by another filtration with UPW. Finally, the ETFE-TMA( $Cl^-$ ) powder was dried at 50 °C in a vacuum oven and milled in a mortar for particle dispersion. The obtained IEC was  $1.97 \pm 0.01 \text{ mmol g}^{-1}$ .

The geometric surface area of GDEs was 5.0  $\text{cm}^2$  and the Pt loadings for anodes and cathodes were  $0.50 \pm 0.03 \text{ mg}_{Pt} \text{ cm}^{-2}$ . Prior to MEA fabrication step, the electrodes and membrane were immersed in a solution of KOH (1 M) for 1 h, followed by washing with water to remove excess  $K^+$  and  $OH^-$  ions. The membrane-electrode assembly (MEA) was assembled by placing the anode, cathode, and the synthesized AEMs ( $4 \times 4 \text{ cm}^2$ ) between two graphite plates with serpentine type distribution channels, applying a torque of 5 N m.

The fuel cell tests were performed in a Scribner Assoc. 850C fuel cell test station. The anode was fed with pure  $H_2$  (99.999%), flow of 0.8  $\text{L min}^{-1}$ , and the cathode with pure  $O_2$  (99.998%), flow of 0.5  $\text{L min}^{-1}$ . The fuel cell was maintained at 80 °C during all experiments and optimal temperatures were found for the humidifiers for each AEM (in a range of 77–80 °C) at ambient pressure.

The chemical stability of the AEMs was obtained by using the same procedure described in 2.2.4 section for  $OH^-$  conductivity. The RH was set to 80% and the cell temperature stabilized at 60 °C. Measurements were carried out at 30 min time intervals during 100 h and a 0.2 mA constant current was applied to avoid carbonation in the AEM. The chemical stability of AEMs was obtained from the loss in the true  $OH^-$  conductivity per hour [40].

### 3. Results and discussion

#### 3.1. AEMs general properties

The LDPE films were grafted using two methods: i) pre-irradiation (PIM), using electron-beam (EB), and ii) simultaneous (SM), using gamma-ray ( $\gamma$ ), both in air atmosphere and with different absorbed doses. The 4-VBC-grafted AEMs by SM were irradiated with 20, 25, and 30 kGy, while the ones grafted by PIM were irradiated with doses of 30, 70, and 100 kGy. Such absorbed doses were chosen in order to obtain AEMs with comparable degree of grafting (DoG) and ion exchange

capacity (IEC), allowing a systematic analysis of the inherent chemical and structural effects introduced by the grafting method (Table S1 shows AEMs with other attempts of absorbed doses for additional information).

Fig. 1a shows DoG and IEC values for TMA-functionalized LDPE-based AEMs produced via PIM and SM. Basically, membranes with similar DoG also have similar IEC, indicating that the synthesis method does not interfere in the IEC parameter, which is directly related to the DoG. It is interesting to note that DoG increases with increasing radiation absorbed dose in a faster rate for samples irradiated by  $\gamma$ -rays (SM), than for the ones irradiated by EB (PIM), as shown in Fig. 1b. In the case of  $\gamma$ -SM samples, DoG rises from 85 to 154% with increasing absorbed dose from 20 to 30 kGy, whereas membranes synthesized by PIM required 30 kGy to reach 80% of DoG and 100 kGy to reach 155%. This happens because in the SM, both the formation of free radicals and the grafting reaction take place concomitantly. Meantime in the PIM, in which only the polymer matrix is exposed to ionizing radiation, the grafting occurs in a further reaction. In this method, free radicals formed in the base polymer react with  $O_2$  in the air to form peroxides and hydroperoxides (see reactions 5 to 7 in Fig. S1), which will be in contact with a non-irradiated monomer solution subsequently.

In the SM, free radicals formed in the monomer solution might also react instantly with each other, forming homopolymers. In this method, both reactions (homopolymerization and grafting) compete depending on the  $\gamma$ -ray dose rate and the medium composition. On the other hand, in the PIM, there is low/no homopolymerization, since the monomer is not irradiated. In this method, during the grafting reaction, peroxides/hydroperoxides undergo decomposition to free radicals (thermally activated), which then initiates grafting; however, not all polymeric radicals will find a monomer molecule to react. Thus, PIM requires more radicals than the SM to achieve the same DoG, demanding higher radiation absorbed doses.

In addition, due to the high energy involved, other competing reactions take place in the polymer backbone itself during irradiation, such as crosslinking and chain scission reactions (please, see Fig. S1), which also affect the grafting yield. These reactions are more pronounced during EB irradiation than during  $\gamma$ -rays due to the differences in absorbed dose rates [17]. Fig. S1 shows the main reactions occurring during both irradiation processes.

Table 1 summarizes additional results obtained from AEMs produced by PIM and SM, such as water uptake (WU), number of water molecules per anion ( $\lambda$ ), and trough-plane swelling (TPS) values. A direct correlation between DoG and IEC results from the ability of both methods (PIM and SM) in promoting equivalent monomer grafting even at different absorbed doses. However, AEMs with similar DoG and IEC, produced by SM and PIM, resulted in distinct WU. AEMs synthesized by

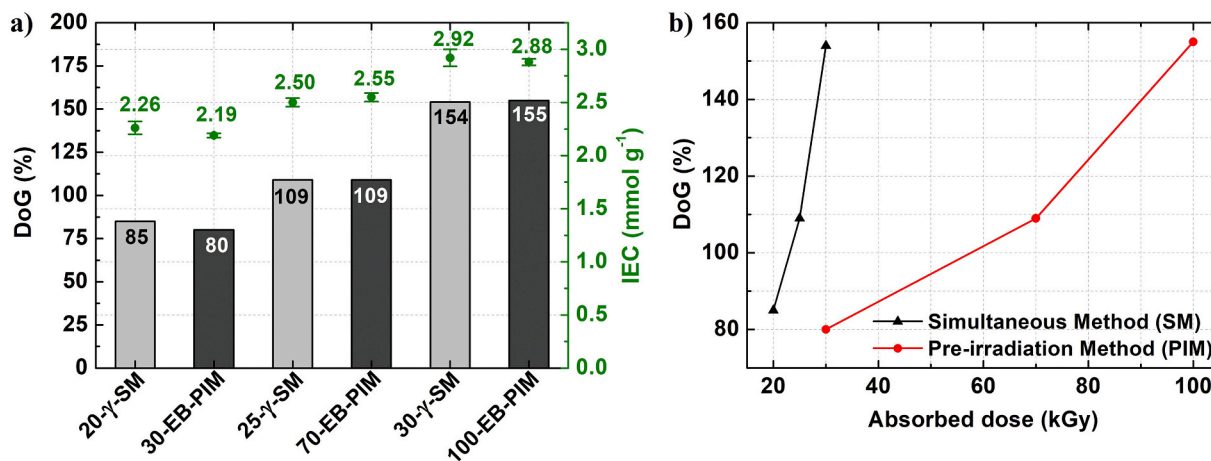


Fig. 1. a) Degree of Grafting (DoG) and Ion Exchange Capacity (IEC) of LDPE-based AEMs grafted by simultaneous method (SM – light grey bars) and pre-irradiation method (PIM – dark grey bars). b) Comparison of DoG vs absorbed dose relation for each method.

SM exhibited higher WU than the corresponding AEMs produced by PIM. The measurements of WU after soaking samples in water at 90 °C for 1 h (Fig. S2) confirm such observations, demonstrating that, differently of DoG and IEC, the water absorption capacity is remarkably dependent on the grafting methodology. This feature also reflected on both  $\lambda$  and TPS values, which are hydration-dependent parameters, evidencing that AEMs with lower WU, EB-PIM AEMs, result in lower  $\lambda$  and TPS than the corresponding  $\gamma$ -SM-AEMs. In summary, the combined experimental data indicate that both grafting methods produce AEMs with equivalent DoG and, consequently, similar IEC, but with distinct properties associated with the water absorption (WU,  $\lambda$ , and TPS).

The observed differences on WU and TPS are possibly related to distinct microstructural properties due to different competitive crosslinking and scission reactions happening during  $\gamma$  and EB irradiations. Crosslinking promotes the formation of a dense three-dimensional polymeric network with an increase in molecular weight [44]. Polymers with high crosslinking density usually retain less water because of low free volume between the polymer chains that decrease the accommodation of water molecules [45]. Such a relation was previously observed by Guiver et al. [46], who demonstrated lower swelling ratios for crosslinked membranes than for uncrosslinked ones. Also, a similar feature was reported by Gao et al. [45] in AEMs showing a gradual decrease in WU and swelling ratio with increasing degree of crosslinking.

The determination of the extent of crosslinking in the different AEMs is essential to understand their intrinsic properties. By calculating the amount of gel in the irradiated-only LDPE films after solvent extraction [38] it was possible to infer the crosslinking in the studied samples. LDPE chains effectively interconnected are not extractable by an adequate solvent such as xylol, while the gel content (GC) is the measure of this non-soluble part of the polymer directly related to the crosslinking [47]. The GC of samples irradiated by  $\gamma$ -rays was determined for films irradiated in air without monomer solution, to avoid any interference of grafted chains. The GC values are listed in Table 2.

The results evidence that the number of crosslinks in irradiated LDPE film samples is considerably higher in the EB-irradiated samples compared to  $\gamma$ -irradiated samples. In addition, GC increases with the absorbed dose, which is related to the formation of a large number of free radicals as the dose increases, with a significant probability of recombination, especially in EB samples. An interesting fact is that films irradiated with  $\gamma$ -rays in air have shown exceptionally low gel content (<11%), even in absence of monomer solution during irradiation. As there were no monomer radicals reacting with the LDPE-backbone, it could be expected some crosslinking between chains, especially at 30 kGy. Samples irradiated with 30 kGy by the two different techniques (irrad-30-EB and irrad-30- $\gamma$ ) reveal how the dose rate affects the extent of the reactions between free radicals formed in the polymer backbone. These radicals are the same type regardless the source of radiation (shown in Fig. S1). However, in  $\gamma$ -rays irradiation, the dose rate is so low, compared to EB, that free radicals rather participate in reversible reactions than recombine, going back to the initial form of the polymeric molecule. This results in lower GC in comparison to the correspondent sample irradiated by EB using the same absorbed dose. It is important to consider that in the monomer solution, in the case of  $\gamma$ -SM AEMs, the crosslinking extent is possibly even lower, due to the competitive

**Table 2**

Gel content (GC) of pristine LDPE and irradiated LDPE films by  $\gamma$ -rays or EB.

Sample	Dose (kGy)	GC (%)
pristine LDPE	–	0
irrad-30-EB	30	42
irrad-70-EB	70	60
irrad-100-EB	100	69
irrad-20- $\gamma$	20	8
irrad-25- $\gamma$	25	11
irrad-30- $\gamma$	30	11

reaction involving monomer free radicals in high concentration.

### 3.2. Molecular structure and grafting homogeneity

Fig. 2a and b show the Raman spectra of LDPE films grafted with 4-VBC and the resulting AEMs functionalized with TMA, respectively.

The spectrum of the pristine LDPE film (Fig. 2a) showed four major peaks at 1440, 1296, 1128, and 1062  $\text{cm}^{-1}$ . The peaks at 1440 and 1296  $\text{cm}^{-1}$  correspond to deformations of the  $\text{CH}_2$  groups, and the ones at 1128 and 1062  $\text{cm}^{-1}$  are related to the C–C stretching modes [26]. When 4-VBC was added to the LDPE backbone - either in the pre-irradiation or simultaneous grafting - new peaks are detected: 1612  $\text{cm}^{-1}$ , characteristic of the vibrations of the aromatic ring of the 4-VBC; 1267  $\text{cm}^{-1}$ , which is related to the  $\text{CH}_2$  wagging mode of the  $\text{CH}_2\text{Cl}$  group; and peaks between 600 and 800  $\text{cm}^{-1}$  due to C–Cl stretches [26]. In the AEMs functionalized with TMA (Fig. 2b) the peak at 1267  $\text{cm}^{-1}$  is absent because the  $-\text{CH}_2\text{Cl}$  group is replaced by the quaternary ammonium group. The TMA-based functional groups were identified by the well-defined bands at 976, 891, and 765  $\text{cm}^{-1}$ , which are associated with cationic trimethylamine groups [7,48]. No remarkable differences were observed between the AEMs synthesized by the different methods, indicating that the molecular structure is preserved independently on the radiation-induced grafting method.

To verify the homogeneity of the films after grafting, Raman mappings across the film thickness were acquired for the samples with the

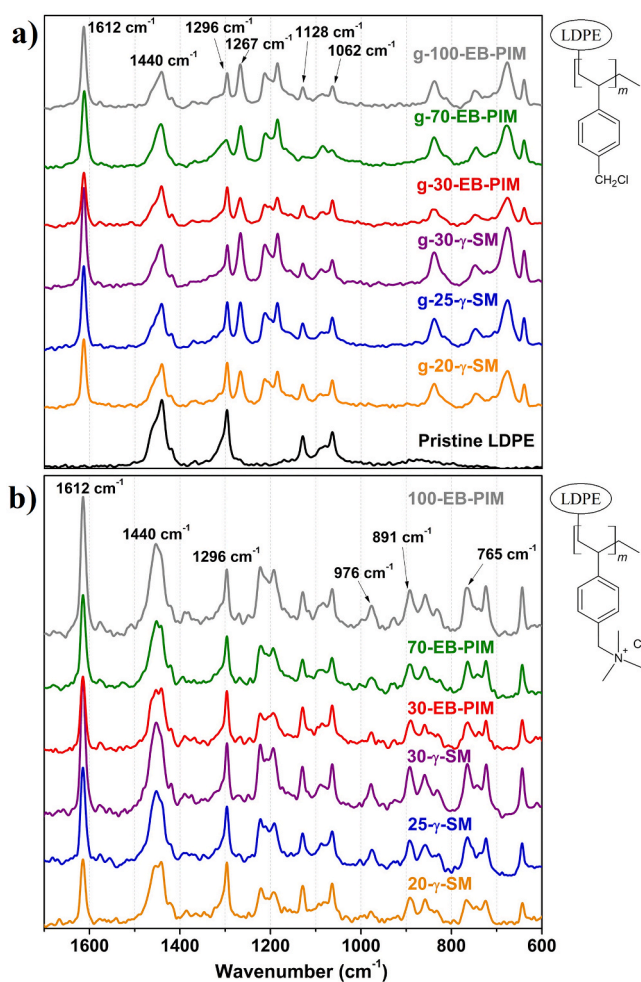


**Fig. 2.** Raman spectra of a) pristine LDPE-film (black line), VBC-grafted LDPE films grafted by the different methods and doses (simultaneous: “ $\gamma$ -SM” samples and pre-irradiation: “g-EB-PIM” samples), and b) final AEMs aminated with TMA. Laser  $\lambda = 1064$  nm.

highest degree of grafting for each method (g-30- $\gamma$ -SM and g-100-EB-PIM samples), as shown in Fig. 3. The colors represent the intensity of the integrated peak area ratio of peaks 1612 and 1128  $\text{cm}^{-1}$ , related to the 4-VBC and LDPE backbone, respectively. It is possible to observe that in both samples, grafting is not homogeneous throughout the thickness, being more concentrated on the surface on both sides. The decreased concentration in the bulk of the films is consistent with the grafting front mechanism [17], in which grafting reaction starts on the surface of the film and, as the reaction takes place, the swelling of the film occurs by a gradient of monomer diffusion that proceeds from surface towards the bulk [49,50]. Such mechanism and the final homogeneity depend on several parameters, such as time of the reaction, solvent, and temperature [51]. In the case of AEMs prepared via SM, a more homogenous grafting is expected due to the low absorbed dose rate (0.5  $\text{kGy h}^{-1}$ ). Such a low dose rate provided by  $\gamma$ -radiation requires longer reaction times for the SM than for the PIM (using EB), thus, the monomer has a longer time to diffuse through the thickness (60 h vs 5 h for SM and PIM, respectively). Besides, toluene in the solvent mixture enhances the accessibility of monomer to the grafting sites through base polymer swelling, favoring bulk grafting [17]. In the PIM, the presence of a very polar solvent (water), which has low solubility for the grafted polymer and low ability to swell the LDPE film, favors the surface grafting despite enhancing grafting kinetics [51]. Additionally, a high degree of crosslinking in these samples can hinder the monomer diffusion resulting in heterogeneous grafting through the thickness of the membrane [17]. Therefore, maps shown in Fig. 3 demonstrate that grafting occurred along the LDPE thickness in both grafting methods, but is more concentrated on the surfaces, a feature more evident in the pre-irradiation method.

### 3.3. Mechanical properties

The mechanical properties of AEMs are crucial to ensure a long-term fuel cell operation. In order to evaluate the effect of the grafting method on the AEM's mechanical properties, tensile tests were carried out as

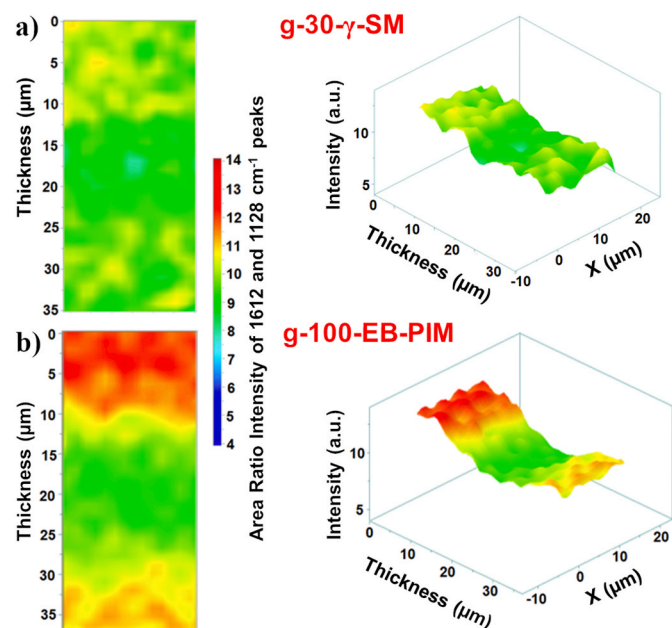


Fig. 3. Raman cross-sectional maps of LDPE films grafted with 4-VBC by a) simultaneous method (g-30- $\gamma$ -SM sample) and b) pre-irradiation method (g-100-EB-PIM sample). The color scale represents the peak area ratio between 1612  $\text{cm}^{-1}$  and 1128  $\text{cm}^{-1}$  Raman peaks (content of benzene rings vs LDPE). (For interpretation of the references to color in this figure legend, the reader is referred to the Web version of this article.)

shown in Fig. 4.

The mechanical behavior of AEMs is affected by both the irradiation – essentially by a competition between formation of crosslinking and chain scission – and the processing steps of grafting and amination. Fig. 4 provides information concerning the influence of both the grafting method and the DoG on the mechanical properties.

By evaluating AEMs with different DoGs synthesized by the PIM it is possible to observe a slight increase in the elastic modulus with increasing radiation dose (Fig. 4a). Such an increase is possibly associated with the rise in the irradiation absorbed dose rather than be related to the amount of monomer grafted to the polymer backbone. This feature is an indication of higher crosslinking density, in good agreement with the GC values, which also increased with the absorbed dose (see Table 2). On the other hand, no significant differences can be noted in the elastic modulus among the 3 SM-AEMs samples, since crosslinking density is very low in all of them, in good agreement with GC values.

By comparing AEMs synthesized by the different methods, PIM and SM, it is possible to observe that EB-PIM AEMs have significantly higher elastic modulus values than those attributed to  $\gamma$ -SM AEMs. Such a higher elastic modulus is consistent with preferential crosslinking reaction in the LDPE backbone of EB-PIM samples, which contribute to the reinforcement of the polymer structure. Analyzing both 30- $\gamma$ -SM and 30-EB-PIM AEMs, in Fig. 4a, it is possible to infer that the chain reinforcement is strongly dependent on the type of irradiation (related to the grafting method) rather than on the amount of absorbed dose. The 30-EB-PIM AEM exhibits an almost threefold increase in elastic modulus compared to the 30- $\gamma$ -SM sample (485 and 189 MPa, respectively) despite having different DoGs. In general, the elastic modulus increases with increasing crosslinking density to a more rigid material. Moreover, an extremely high crosslinking density can produce a fragile final material, reducing its elongation capacity.

On the contrary, the elongation at break of AEMs under study (Fig. 4b) shows a less pronounced dependence on the grafting method. Despite the appreciable difference in the elastic modulus between EB-PIM and  $\gamma$ -SM samples, the variation in elongation at break values is less evident. This indicates that the reinforcement provided by the crosslinking in EB-PIM AEMs did not make the samples fragile, preserving their elongation capacity. Thus, the behavior of elongation at break and the values of elastic modulus indicate that EB-PIM AEMs have enhanced mechanical properties compared to  $\gamma$ -SM AEMs.

### 3.4. Microstructure

The degree of crosslinking in the membrane and, consequently, the water absorption and the mechanical properties are strictly related to the microstructural modification in the LDPE films resulting from the processing method. The AEM morphology determines water distribution, size of ionic clusters, and the interface between hydrophilic and hydrophobic domains. Such features, in turn, influence the water and ion transport processes in the AEM [52].

In order to understand the differences in the microstructure between EB-PIM and  $\gamma$ -SM-AEMs, SAXS measurements were performed in dry samples. The long-distance period (D) is known as the sum of the crystalline and amorphous layer thickness of LDPE and can be calculated through the maximum scattering of the SAXS profile ( $D = 2\pi/q$ ) [53], indicating microphase-segregation. Therefore, SAXS analysis were based on the eventual variations on D parameter.

Fig. 5 presents the Lorentz corrected SAXS profiles of the pristine LDPE and resulting AEMs. The typical pristine LDPE long-distance period peak appears around  $q = 0.052 \text{ \AA}^{-1}$  ( $D_1 = 12.0 \text{ nm}$ ). On the other hand, the EB-PIM-AEMs, Fig. 5a, show a long-distance period peak displacement to higher angles,  $q \sim 0.058 \text{ \AA}^{-1}$ , and a decrease in intensity compared to the pristine LDPE film. The peak shift towards higher angles is associated to the reduction of the  $D_1$  sizes,  $D_1 = 11.0 \text{ nm}$  for 30 and 70-EB-PIM AEMs and  $D_1 = 10.7 \text{ nm}$  for 100-EB-PIM AEM, and the intensity reduction is associated to an alteration in concentration of

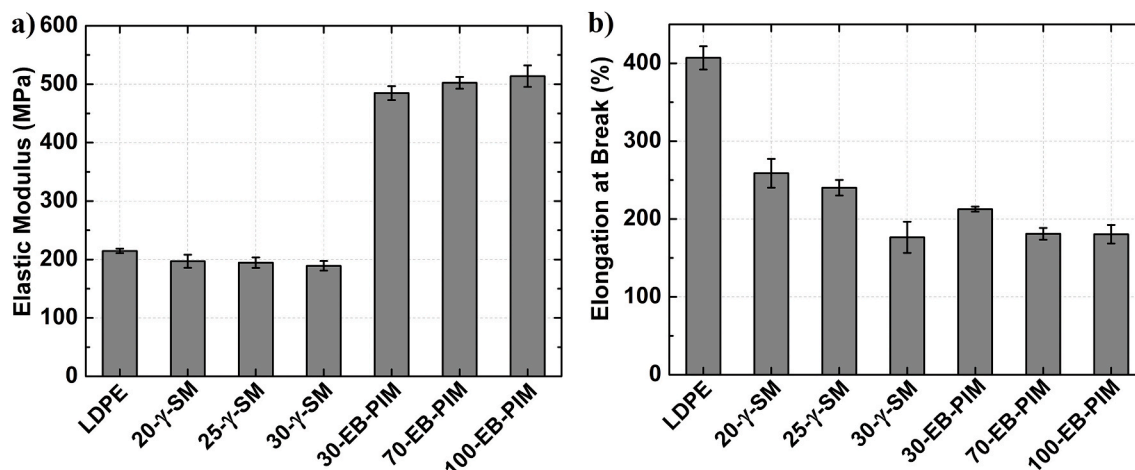


Fig. 4. Mechanical properties of pristine LDPE film; radiation-grafted AEMs prepared by the simultaneous method (20- $\gamma$ -SM, 25- $\gamma$ -SM, and 30- $\gamma$ -SM); and by the pre-irradiation method (30-EB-PIM, 70-EB-PIM, and 100-EB-PIM): a) Elastic Modulus; b) Elongation at break.

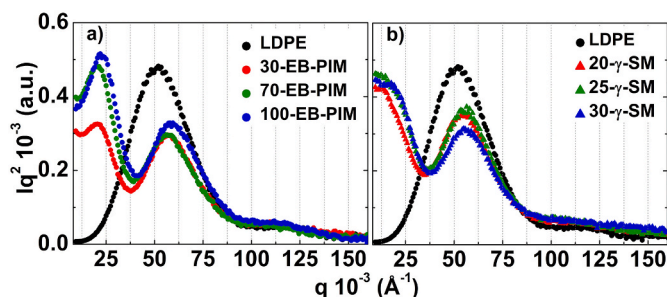


Fig. 5. Lorentz corrected SAXS profiles of pristine LDPE (black lines) and AEMs a) grafted by the pre-irradiation method and b) grafted by the simultaneous method.

lamellar structures and amorphous phase. Furthermore, in the EB-PIM-AEMs, it is possible to observe a new and sharp peak at low angles ( $q \sim 0.022 \text{ \AA}^{-1}$ ) indicating the formation of a new phase separation introduced by synthesis steps. This new peak seems to be related to the ionic domains of the AEMs, since the addition of quaternary ammonium groups, linked to poly(VBC) chains, introduces hydrophilic character to the AEM. The phase separation between hydrophobic and hydrophilic domains is important for the transportation of  $\text{OH}^-$  ions. Well-connected hydrophilic domains normally facilitate the ion conduction, while the hydrophobic phase is responsible for the mechanical stability of the membrane [52]. The low angle interdomain distances ( $D_2$ ) are  $\sim 3$  times larger than the typical LDPE long-distance period. Similar sizes were found for hydrophilic domains of AEMs by Jae-Hong Choi et al. [54] (30 nm), Pepa Cotanda et al. [55] (26–63 nm), and Qiang Zhang et al. (20–30 nm) [56]. This is in agreement with the fact that anions need a larger domain size to be transported in comparison with  $\text{H}^+$ , without being obstructed by hydrophobic phases [52].

The  $\gamma$ -SM AEMs, Fig. 5b, as well as EB-PIM-AEMs, show the LDPE-related long-distance period peak shifted to higher angles, which means a decrease in the long-distance periods' sizes ( $q \sim 0.056 \text{ \AA}^{-1}$ ,  $D_1 = 11.3$  for all  $\gamma$ -SM-AEMs) compared to pristine LDPE film ( $D_1 = 12.0$  nm). Nonetheless, in  $\gamma$ -SM AEMs, the low angle peak,  $q < 0.025 \text{ \AA}^{-1}$ , is much less intense and less distinguishable when compared to EB-PIM-AEMs. Thus, the difference in this peak between  $\gamma$ -SM and EB-PIM AEMs shows unequivocally a correlation between sample morphology and grafting method. In this context, Fig. 6 shows possible microstructures of  $\gamma$ -SM and EB-PIM AEMs and their respective  $D_1$  and  $D_2$ . In this representation, it can be observed that ionic domains appear to be more organized in EB-PIM AEMs than in  $\gamma$ -SM AEMs. In EB-PIM samples, the higher

concentration of scattering centers, generates a more pronounced scattering peak.

The contrasts observed in the microstructure of both types of AEMs can be explained by the differences in degree of crosslinking and grafting homogeneity. Additionally, the arrangement of ionic groups across the membranes is primarily associated with the AEM microstructure and influences both water and ions transport mechanisms. Therefore, the variation in morphology will certainly allow water to be distributed differently in both types of AEMs during fuel cell operation.

### 3.5. Electrochemical properties

Fig. 7a and b show the ionic conductivity data as a function of temperature,  $\sigma(T)$ , of AEMs in  $\text{Cl}^-$  form at RH = 100%. The  $\sigma(T)$  exhibits a thermally activated behavior and the IEC has a direct dependence on  $\sigma$  of the AEMs. Samples with similar IEC, synthesized by the two different methods, display comparable  $\sigma$  (see Fig. S3 for better visualization) and increasing the IEC increases the AEMs  $\sigma$ . The plots of  $\ln \sigma$  ( $\text{S cm}^{-1}$ ) versus  $1000/T$  (temperature in Kelvin), Fig. S4, follow an Arrhenius behavior [57]. The calculated activation energies ( $E_a$ ) [58] of AEMs in the  $\text{Cl}^-$  form varied from 13.9 to 16.6  $\text{kJ mol}^{-1}$  and are listed in Fig. S4. Interestingly, the  $\sigma$  dependence on the IEC differs when substituting the transported anion  $\text{Cl}^-$  for  $\text{OH}^-$ , as shown in Fig. 7c. In  $\text{OH}^-$  form, AEMs with similar IECs (25- $\gamma$ -SM and 70-EB-PIM) have shown different  $\sigma$ , such as 220 and 240  $\text{mS cm}^{-1}$  at 80  $^\circ\text{C}$ , respectively. These values are among the highest hydroxide conductivities reported for similar AEMs, please see Table S2. It is worth mentioning that measurements in  $\text{OH}^-$  are normally affected by the  $\text{CO}_2$  in air, promoting the formation of  $\text{HCO}_3^-/\text{CO}_3^{2-}$  [59]. To avoid any carbonation, a constant voltage of 0.5 V was applied during all the experiments [40–42]. In such condition, hydroxide ions are produced at the cathode by water splitting and the generated ions purge out the bicarbonate species in form of  $\text{CO}_2$ , which enables the AEM to be in its fully  $\text{OH}^-$  form [42]. The obtained values of  $E_a$  for AEMs in  $\text{OH}^-$  form were 11.7 and 12.8  $\text{kJ mol}^{-1}$ , for 70-EB-PIM and 25- $\gamma$ -SM AEMs, respectively, similar to what is found in the literature for TMA functionalized AEMs [60,61]. The slight difference in  $E_a$  for hydroxide diffusion between these two AEMs may be related to their distinct hydration number ( $\lambda$ ) [57].

The observed contrasts between  $\text{Cl}^-$  and  $\text{OH}^-$  conductivities can be explained by the fact that the  $\text{OH}^-$  groups are transported by two mechanisms in the membrane, while  $\text{Cl}^-$  is shuttled only by one. The vehicular mechanism (i), where the ion moves between ammonium groups by diffusion/migration or convection [62], is available for  $\text{OH}^-$  and  $\text{Cl}^-$  ions. Meantime, Grothuss mechanism (ii) is only accessible for  $\text{OH}^-$ , in which this ion is transported through O–H bond breaking and

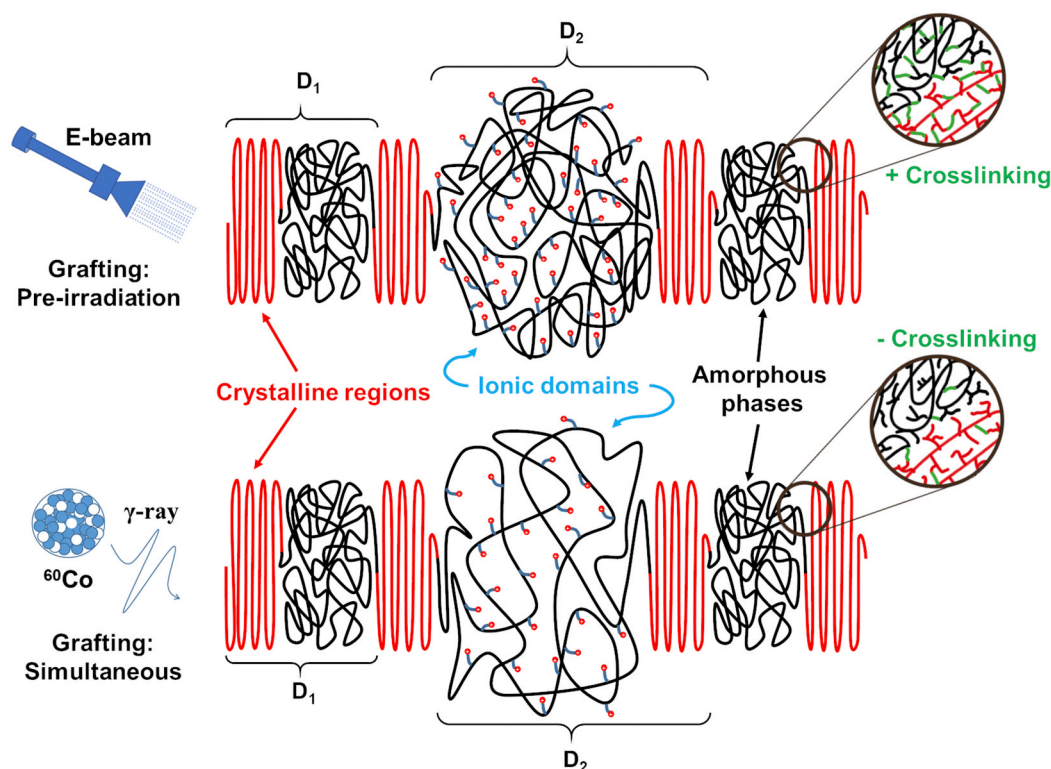


**Fig. 6.** Simplified morphology representation of AEMs synthesized by the pre-irradiation method (top) and by the simultaneous method (bottom).  $D_1$  represents the long-distance period size related to the LDPE structure and  $D_2$  is related to the ionic domains' size. Zooms in the drawings show the LDPE branching and crosslinking between chains.

formation with water molecules [63,64], demanding lower activation energy than in (i). Both mechanisms are strongly dependent on the amount of water in the membrane; however, too high hydration levels can result in a decrease in the charge carriers' density [65]. The microstructural properties of the AEM also play an important role in ion transport [62], facilitating or inhibiting the above-mentioned mechanisms. In this context, the water uptake and the morphology of the AEMs can affect the hydroxide conductivity despite of similar IECs. On the other hand, as  $\text{Cl}^-$  is shuttled only via vehicular mechanism [61], the conductivity does not seem to be affected by the AEM synthesis method. In this case, the most important property affecting this parameter is the amount of QAs present in the sample, therefore, the IEC. When comparing samples irradiated with the same dose and prepared by the two different methods (30-EB-PIM and 30- $\gamma$ -SM AEMs), it is evident that the ionic conductivity is not related to the absorbed dose, but to the number of functional groups in the membrane. Thus, considering the same absorbed dose, the ion conductivity depends on the grafting methodology used.

One of the goals of this work is to gather experimental evidence that can lead to a better understanding of the influence of the grafting method on the fundamental physicochemical properties of AEMs, which imply in the performance and durability of fuel cells. In this context, Fig. 8 shows the polarization curves of AEMFCs operating at 80 °C with AEMs grafted by PIM and SM. By analyzing the AEMs produced via PIM (Fig. 8a), it is possible to notice that AEMFCs containing 30-EB-PIM and 100-EB-PIM AEMs have the same polarization profile, which results in a quite similar maximum power density (differing by less than 0.1 W  $\text{cm}^{-2}$ ). On the other hand, 70-EB-PIM AEM presents the best performance ( $\sim 1.43$  W  $\text{cm}^{-2}$ ) with an apparent variation on both ohmic and mass transport mechanisms.

The polarization curves obtained from AEMFCs containing AEMs produced via SM (Fig. 8b) reveal the same polarization profile evidenced for the ones assembled with EB-PIM AEMs, 20- $\gamma$ -SM and 30- $\gamma$ -SM

samples, have similar polarization curves and performances, while 25- $\gamma$ -SM differed in the mass transport and ohmic polarization regions. It is interesting to note that, for both synthesis methods, membranes with intermediate IEC values have shown the highest maximum power density, 1.43 and 1.24 W  $\text{cm}^{-2}$  for 70-EB-PIM and 25- $\gamma$ -SM, respectively. Such a behavior can be explained taking into account that both ohmic drop and mass transport are water-dependent processes.

The water management in AEMFCs is complex and involves a delicate balance between anode flooding and cathode dry out. For each reacting oxygen, four molecules of water are produced at the anode, and two are consumed at the cathode [66]. Besides that, the movement of  $\text{OH}^-$  ions from the cathode brings more water to the anode by electro-osmotic drag. Therefore, the polarization data is closely related to the water absorption capacity of each AEM and water management. AEMs with very high IECs are probably experiencing ohmic losses and mass transport limitations due to the high hydration levels. Such high humidity makes the fuel cell more prone to anode flooding. On the other hand, polarization losses of fuel cells containing low IEC AEMs are probably due to cathode (and anode) dry out. Thus, AEMs with intermediate IECs handle better the water management and allow to reach higher current densities in a certain potential range.

Comparing AEMFCs performances containing AEMs from the two different grafting methods, it is possible to notice that AEMs synthesized by PIM, in general, promote better fuel cell performances than the corresponding ones prepared by SM (see Fig. S5 for better visualization). Considering that the electrodes are the same in all AEMFCs, no appreciable variation on the activation polarization region is observed. The main differences are evidenced in the ohmic and the mass transport limiting regions of the polarization curves. This result suggests better water management by AEMs synthesized by PIM than by SM. Many factors influence the water balance/imbalance, such as the gas flow, dew points, fuel cell temperature, gas diffusion layer, ionomer in the catalyst layer, and the membrane morphology itself [66–69]. A membrane that

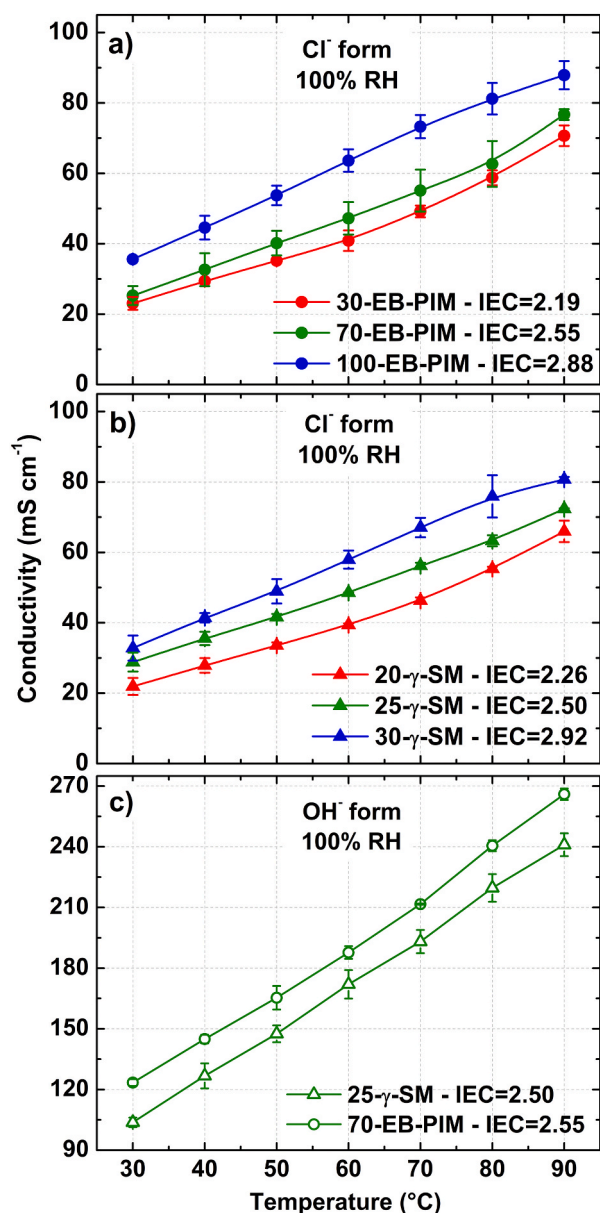


Fig. 7. Temperature dependence of the ionic conductivity at RH100% of AEMs synthesized by a) pre-irradiation method and b) by simultaneous method in Cl<sup>-</sup> form; c) example of two AEMs in OH<sup>-</sup> form (the standard deviation bars for 70-EB-PIM are very small and in some points they appear overlapping or inside the data circles).

allows rapid back diffusion of liquid water from the anode to the cathode, should reduce the current losses due to mass transport limitations.

The fuel cell data confirm what was observed by SAXS, showing that the differences in morphology between AEMs synthesized by the two different methods directly influence the performance of the AEMFCs. This influence seems to be related to the arrangement of ionic groups across the membranes and the way water is transported through them. However, more studies are needed to provide a structural model and understand how water transport actually takes place.

Finally, *ex-situ* short-term stability tests were carried out for 70-EB-PIM and 25- $\gamma$ -SM AEMs in order to observe the impact of grafting methodology on this property, Fig. S6. The stability measurements followed a recently reported method [40,41] to accurately infer the true hydroxide conductivity. The true hydroxide conductivity was measured for 100 h at 60 °C and RH = 80%. Interestingly, the results show the same conductivity decay for both AEMs (0.14% h<sup>-1</sup>) indicating that the

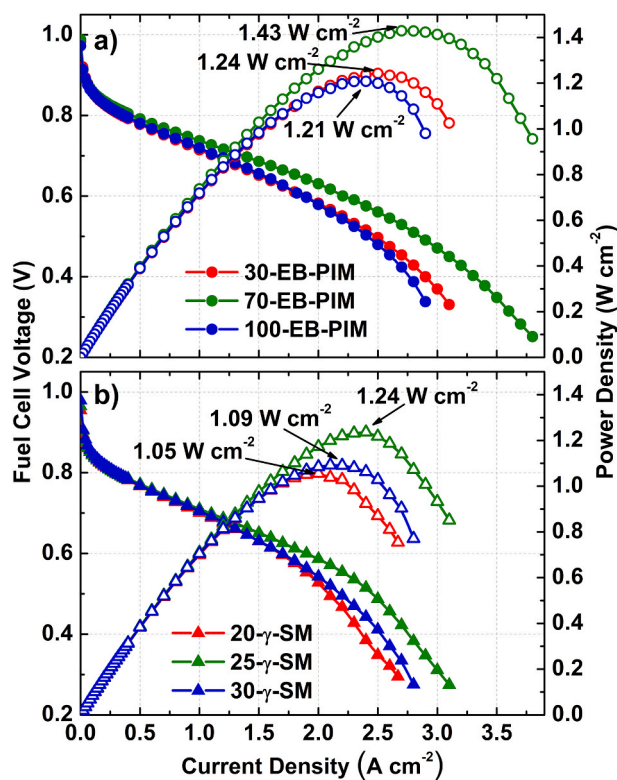


Fig. 8. AEMFCs performances at 80 °C with a) LDPE-based AEMs grafted by the pre-irradiation method and b) AEMs grafted by the simultaneous method. H<sub>2</sub> anode gas flow = 0.8 L min<sup>-1</sup>, O<sub>2</sub> cathode gas flow = 0.5 L min<sup>-1</sup>, both supplied unpressurized with optimal dewpoint temperatures ranging from 77 to 80 °C.

synthesis method seems to not influence the chemical stability in short-term tests (see Fig. S6 for the normalized true OH<sup>-</sup> conductivity as function of time). This conductivity decay is relatively low considering similar AEMs in the literature, please see Table S2. Most of the reported studies use 100% RH for the stability tests, which is less demanding for the AEM. J. Müller et al. [40] tried to simulate more critical conditions in an LDPE-TMA AEM by using 60% RH at 80 °C and obtained a 0.4% h<sup>-1</sup> decay. The same membrane in 100% RH had a 0.07% h<sup>-1</sup> decay of ionic conductivity. However, it is worth noting that mechanical failure would be likely to occur after long periods of operation [70]. Such a feature is directly linked to the swelling capacity, as well as the mechanical properties of the membranes. In this regard, membranes synthesized by PIM seem to be more advantageous due to the high degree of crosslinking compared to membranes synthesized by SM, contributing to backbone reinforcement and consequently to AEM mechanical stability and long-term durability.

#### 4. Conclusions

The impact of the radiation-induced grafting method on the physicochemical properties of LDPE-based anion-exchange membranes with the same molecular structure was studied in detail. The results confirmed the presence of more crosslinking in membranes synthesized by the pre-irradiation method (PIM) when compared to the ones synthesized by the simultaneous method (SM). AEMs with similar DoG and IEC were evaluated to understand the influence of crosslinking in the polymer matrix on the final properties of LDPE-based AEMs. Enhanced mechanical properties for AEMs synthesized by PIM indicate polymer backbone reinforcement due to a high degree of crosslinking. EB-PIM-AEMs have shown better AEMFCs performances than  $\gamma$ -SM-AEMs, which was attributed to the enhanced water mobility. SAXS

measurements have confirmed that the microstructure of EB-PIM and  $\gamma$ -SM AEMs are different and this feature is directly related to ion conduction and water transportation. The water transportation in this type of AEMs still needs further studies, however, the results indicate that AEMs possessing similar DoGs, IECs, and  $\text{Cl}^-$  conductivity will not necessarily have similar fuel cell performances or same mechanical stability, since the grafting step directly influences the internal structure and morphology.

### CRedit authorship contribution statement

**Ana Laura G. Biancolli:** Conceptualization, Data curation, Investigation, Validation, Methodology, Visualization, Writing – original draft, Writing – review & editing. **Andrey S. Barbosa:** Data curation, Investigation, Writing – review & editing. **Yasko Kodama:** Data curation, Investigation, Writing – review & editing. **Rogério R. de Sousa:** Data curation, Investigation, Writing – review & editing. **Alexandre J.C. Lanfredi:** Investigation, Resources. **Fabio C. Fonseca:** Funding acquisition, Resources, Writing – review & editing. **José Fernando Q. Rey:** Investigation, Writing – review & editing. **Elisabete I. Santiago:** Conceptualization, Funding acquisition, Project administration, Resources, Supervision, Writing – original draft, Writing – review & editing.

### Declaration of competing interest

The authors declare that they have no known competing financial interests or personal relationships that could have appeared to influence the work reported in this paper.

### Acknowledgements

The authors are grateful for the support of the Center for Innovation on New Energies (CINE) - SHELL (ANP)/FAPESP grant No. 2017/11937-4, and the Brazilian Nuclear Energy Commission (CENEN). Thanks are also due to the funding support FAPESP No. 2014/09087-4 and ALGB acknowledges the funding support FAPESP No. 2019/26955-3. The authors would like to acknowledge the financial support from International Atomic Energy Agency, research project contract: IAEA RC 23708 and Eng. Elisabete S. Somessari and Eng. Heitor Gameiro Duarte for irradiation of LDPE-films. The authors are grateful to Dr. Rodrigo Moraes Menezes dos Santos for SAXS measurements performed at the SAXS EMU/IQ- UNESP in Araraquara, SP, and to UFABC's Multiuser Central Facility (CEM/UFABC) for access to the Raman equipment. FCF and EIS are research fellows of the Brazilian CNPq.

### Appendix A. Supplementary data

Supplementary data to this article can be found online at <https://doi.org/10.1016/j.jpowsour.2021.230484>.

### References

- [1] D.R. Dekel, Review of cell performance in anion exchange membrane fuel cells, *J. Power Sources* 375 (2018) 158–169, <https://doi.org/10.1016/j.jpowsour.2017.07.117>.
- [2] V. Vijayakumar, S.Y. Nam, Recent advancements in applications of alkaline anion exchange membranes for polymer electrolyte fuel cells, *J. Ind. Eng. Chem.* 70 (2019) 70–86, <https://doi.org/10.1016/j.jiec.2018.10.026>.
- [3] T.B. Ferriday, P.H. Middleton, Alkaline fuel cell technology - a review, *Int. J. Hydrogen Energy* 46 (35) (2021) 18489–18510, <https://doi.org/10.1016/j.ijhydene.2021.02.203>.
- [4] G.O. Larrazábal, P. Strøm-Hansen, J.P. Heli, K. Zeiter, K.T. Therkildsen, I. Chorkendorff, B. Seger, Analysis of mass flows and membrane cross-over in CO<sub>2</sub> reduction at high current densities in an MEA-type electrolyzer, *ACS Appl. Mater. Interfaces* 11 (44) (2019) 41281–41288, <https://doi.org/10.1021/acsaami.9b13081>.
- [5] D. Henkensmeier, M. Najibah, C. Harms, J. Žitka, J. Hnát, K. Bouzek, Overview: state-of-the-art commercial membranes for anion exchange membrane water electrolysis, *J. Electrochem. Energy Convers. Storage* 18 (2) (2021), <https://doi.org/10.1115/1.4047963>.
- [6] J.R. Varcoe, R.C.T. Slade, An electron-beam-grafted ETFE alkaline anion-exchange membrane in metal-cation-free solid-state alkaline fuel cells, *Electrochem. Commun.* 8 (5) (2006) 839–843, <https://doi.org/10.1016/j.elecom.2006.03.027>.
- [7] A.L. Gonçalves Biancolli, D. Herranz, L. Wang, G. Stehliková, R. Bance-Soualhi, J. Ponce-González, P. Ocón, E.A. Ticianelli, D.K. Whelligan, J.R. Varcoe, E. I. Santiago, ETFE-based anion-exchange membrane ionomer powders for alkaline membrane fuel cells: a first performance comparison of head-group chemistry, *J. Mater. Chem. A* 6 (47) (2018) 24330–24341, <https://doi.org/10.1039/C8TA08309F>.
- [8] L. Wang, X. Peng, W.E. Mustain, J.R. Varcoe, Radiation-grafted anion-exchange membranes: the switch from low- to high-density polyethylene leads to remarkably enhanced fuel cell performance, *Energy Environ. Sci.* 12 (5) (2019) 1575–1579, <https://doi.org/10.1039/c9ee00331b>.
- [9] R. Espiritu, B.T. Golding, K. Scott, M. Mamlouk, Degradation of radiation grafted anion exchange membranes tethered with different amine functional groups via removal of vinylbenzyl trimethylammonium hydroxide, *J. Power Sources* 375 (2018) 373–386, <https://doi.org/10.1016/j.jpowsour.2017.07.074>.
- [10] R. Espiritu, B.T. Golding, K. Scott, M. Mamlouk, Degradation of radiation grafted hydroxide anion exchange membrane immersed in neutral pH: removal of vinylbenzyl trimethylammonium hydroxide due to oxidation, *J. Mater. Chem. A* 5 (3) (2017) 1248–1267, <https://doi.org/10.1039/c6ta08232g>.
- [11] A.D. Mohanty, S.E. Tignor, J.A. Krause, Y.K. Choe, C. Bae, Systematic alkaline stability study of polymer backbones for anion exchange membrane applications, *Macromolecules* 49 (9) (2016) 3361–3372, <https://doi.org/10.1021/acs.macromol.5b02550>.
- [12] K. Yang, X. Chu, X. Zhang, X. Li, J. Zheng, S. Li, N. Li, T.A. Sherazi, S. Zhang, The effect of polymer backbones and cation functional groups on properties of anion exchange membranes for fuel cells, *J. Membr. Sci.* 603 (February) (2020) 118025, <https://doi.org/10.1016/j.memsci.2020.118025>.
- [13] J.R. Varcoe, P. Atanassov, D.R. Dekel, A.M. Herring, M.A. Hickner, P.A. Kohl, A. R. Kucernak, W.E. Mustain, K. Nijmeijer, K. Scott, T. Xu, L. Zhuang, Anion-exchange membranes in electrochemical systems, *Energy Environ. Sci.* 7 (10) (2014) 3135–3191, <https://doi.org/10.1039/c4ee01303d>.
- [14] Z.F. Pan, L. An, T.S. Zhao, Z.K. Tang, Advances and challenges in alkaline anion exchange membrane fuel cells, *Prog. Energy Combust. Sci.* 66 (2018) 141–175, <https://doi.org/10.1016/j.peccs.2018.01.001>.
- [15] M.M. Nasef, S.A. Gürsel, D. Karabelli, O. Güven, Radiation-grafted materials for energy conversion and energy storage applications, *Prog. Polym. Sci.* 63 (2016) 1–41, <https://doi.org/10.1016/j.progpolymsci.2016.05.002>.
- [16] K. Dawes, L.C. Glover, D.A. Vroom, The effects of electron beam and G-irradiation on polymeric materials, in: *Physical Properties of Polymers Handbook*, 2007, pp. 867–887, [https://doi.org/10.1007/978-0-387-69002-5\\_52](https://doi.org/10.1007/978-0-387-69002-5_52).
- [17] S. Alkan Gürsel, L. Gubler, B. Gupta, G.G. Scherer, Radiation grafted membranes, *Adv. Polym. Sci.* 215 (1) (2008) 157–217, [https://doi.org/10.1007/12\\_2008\\_153](https://doi.org/10.1007/12_2008_153).
- [18] R. Espiritu, M. Mamlouk, K. Scott, Study on the effect of the degree of grafting on the performance of polyethylene-based anion exchange membrane for fuel cell application, *Int. J. Hydrogen Energy* 41 (2) (2016) 1120–1133, <https://doi.org/10.1016/j.ijhydene.2015.10.108>.
- [19] L. Wang, M. Bellini, H.A. Miller, J.R. Varcoe, A high conductivity ultrathin anion-exchange membrane with 500+ h alkali stability for use in alkaline membrane fuel cells that can achieve 2 W Cm<sup>-2</sup> at 80 °C, *J. Mater. Chem. A* 6 (31) (2018) 15404–15412, <https://doi.org/10.1039/c8ta04783a>.
- [20] T.A. Sherazi, J. Yong Sohn, Y. Moo Lee, M.D. Guiver, Polyethylene-based radiation grafted anion-exchange membranes for alkaline fuel cells, *J. Membr. Sci.* 441 (2013) 148–157, <https://doi.org/10.1016/j.memsci.2013.03.053>.
- [21] A.J. Peacock, *Handbook Polyethylene: Structures, Properties, and Applications*, I., vol. 15, Marcel Dekker, New York, NY, 2000 [https://doi.org/10.1016/0167-188X\(89\)90104-3](https://doi.org/10.1016/0167-188X(89)90104-3).
- [22] L.M. Ferreira, J.P. Leal, M.H. Casimiro, C. Cruz, J.J.H. Lancastre, A.N. Falcão, Evidence of structural order recovery in LDPE based copolymers prepared by gamma irradiation, *Radiat. Phys. Chem.* 94 (1) (2014) 31–35, <https://doi.org/10.1016/j.radphyschem.2013.06.031>.
- [23] M. Mamlouk, J.A. Horsfall, C. Williams, K. Scott, Radiation grafted membranes for superior anion exchange polymer membrane fuel cells performance, *Int. J. Hydrogen Energy* 37 (16) (2012) 11912–11920, <https://doi.org/10.1016/j.ijhydene.2012.05.117>.
- [24] T. Zhou, R. Shao, S. Chen, X. He, J. Qiao, J. Zhang, A review of radiation-grafted polymer electrolyte membranes for alkaline polymer electrolyte membrane fuel cells, *J. Power Sources* 293 (2015) 946–975, <https://doi.org/10.1016/j.jpowsour.2015.06.026>.
- [25] M.M. Nasef, Radiation-grafted membranes for polymer electrolyte fuel cells: current trends and future directions, *Chem. Rev.* 114 (24) (2014) 12278–12329, <https://doi.org/10.1021/cr4005499>.
- [26] L. Wang, J.J. Brink, Y. Liu, A.M. Herring, J. Ponce-González, D.K. Whelligan, J. R. Varcoe, Non-fluorinated pre-irradiation-grafted (peroxidated) LDPE-based anion-exchange membranes with high performance and stability, *Energy Environ. Sci.* 10 (10) (2017) 2154–2167, <https://doi.org/10.1039/c7ee02053h>.
- [27] A. Ashfaq, M.-C. Clochard, X. Coqueret, C. Dispenza, M.S. Driscoll, P. Ulański, M. Al-Sheikhly, Polymerization reactions and modifications of polymers by ionizing radiation, *Polymers* 12 (12) (2020) 2877, <https://doi.org/10.3390/polym12122877>.
- [28] L. Gubler, Polymer design strategies for radiation-grafted fuel cell membranes, *Adv. Energy Mater.* 4 (3) (2014) 1300827, <https://doi.org/10.1002/aenm.201300827>.

- [29] K.M. Meek, C.M. Reed, B. Pivovar, K.D. Kreuer, J.R. Varcoe, R. Bance-Soualhi, The Alkali Degradation of LDPE-Based Radiation-Grafted Anion-Exchange Membranes Studied Using Different *ex Situ* Methods, *RSC Adv.* 10 (60) (2020) 36467–36477, <https://doi.org/10.1039/d0ra06484j>.
- [30] R. Shimura, Y. Suematsu, H. Horiuchi, S. Takeoka, A. Oshima, M. Washio, Fabrication of thermo-responsive cell-culture membranes with poly(N-isopropylacrylamide) by electron-beam graft polymerization, *Radiat. Phys. Chem.* (2020) 171, <https://doi.org/10.1016/j.radphyschem.2020.108741>. October 2019.
- [31] C. Dispenza, S. Alessi, J. Spadaro, *Radiation Processing of Polymers in Aqueous Media. Applications of Ionizing Radiation in Materials Processing*, 2017.
- [32] M.M. Nasef, E.-S.A.S.A. Hegazy, Preparation and applications of ion exchange membranes by radiation-induced graft copolymerization of polar monomers onto non-polar films, *Prog. Polym. Sci.* 29 (6) (2004) 499–561, <https://doi.org/10.1016/j.progpolymsci.2004.01.003>.
- [33] R.L. Clough, High-energy radiation and polymers: a review of commercial processes and emerging applications, *Nucl. Instrum. Methods Phys. Res. Sect. B Beam Interact. Mater. Atoms* 185 (1–4) (2001) 8–33, [https://doi.org/10.1016/S0168-583X\(01\)00966-1](https://doi.org/10.1016/S0168-583X(01)00966-1).
- [34] A. Bhattacharya, B.N. Misra, Grafting: a versatile means to modify polymers: techniques, factors and applications, *Prog. Polym. Sci.* 29 (8) (2004) 767–814, <https://doi.org/10.1016/j.progpolymsci.2004.05.002>.
- [35] L. Wang, E. Magliocca, E.L. Cunningham, W.E. Mustain, S.D. Poynton, R. Escudero-Cid, M.M. Nasef, J. Ponce-González, R. Bance-Soualhi, R.C.T. Slade, D. K. Whelligan, J.R. Varcoe, An optimised synthesis of high performance radiation-grafted anion-exchange membranes, *Green Chem.* 19 (3) (2017) 831–843, <https://doi.org/10.1039/c6gc02526a>.
- [36] Y. Zheng, U. Ash, R.P. Pandey, A.G. Ozioko, J. Ponce-González, M. Handl, T. Weissbach, J.R. Varcoe, S. Holdcroft, M.W. Liberatore, R. Hiesgen, D.R. Dekel, Water uptake study of anion exchange membranes, *Macromolecules* 51 (9) (2018) 3264–3278, <https://doi.org/10.1021/acs.macromol.8b00034>.
- [37] D. Manas, M. Ovsik, A. Mizera, M. Manas, L. Hylova, M. Bednarik, M. Stanek, The effect of irradiation on mechanical and thermal properties of selected types of polymers, *Polymers* 10 (2) (2018), <https://doi.org/10.3390/polym10020158>.
- [38] ASTM D2765-16, Standard Test Methods for Determination of Gel Content and Swell Ratio of Crosslinked Ethylene Plastics, ASTM International, West Conshohocken, PA, 2016, <https://doi.org/10.1520/D2765-16>.
- [39] B.R. Matos, C.A. Goulart, E.I. Santiago, R. Muccillo, F.C. Fonseca, Proton conductivity of perfluorosulfonate ionomers at high temperature and high relative humidity, *Appl. Phys. Lett.* 104 (9) (2014), <https://doi.org/10.1063/1.4867351>.
- [40] J. Müller, A. Zhegur, U. Kreuer, J.R. Varcoe, D.R. Dekel, Practical *ex-situ* technique to measure the chemical stability of anion-exchange membranes under conditions simulating the fuel cell environment, *ACS Mater. Lett.* 2 (2) (2020) 168–173, <https://doi.org/10.1021/acsmaterialslett.9b00418>.
- [41] A. Zhegur-Khais, F. Kubannek, U. Kreuer, D.R. Dekel, Measuring the true hydroxide conductivity of anion exchange membranes, *J. Membr. Sci.* 612 (June) (2020) 118461, <https://doi.org/10.1016/j.memsci.2020.118461>.
- [42] X. Cao, D. Novitski, S. Holdcroft, Visualization of hydroxide ion formation upon electrolytic water splitting in an anion exchange membrane, *ACS Mater. Lett.* 1 (3) (2019) 362–366, <https://doi.org/10.1021/acsmaterialslett.9b00195>.
- [43] T.J. Omasta, Y. Zhang, A.M. Park, X. Peng, B. Pivovar, J.R. Varcoe, W.E. Mustain, Strategies for reducing the PGM loading in high power AEMFC anodes, *J. Electrochem. Soc.* 165 (9) (2018) F710–F717, <https://doi.org/10.1149/2.1401809jes>.
- [44] T. Huang, G. He, J. Xue, O. Otoo, X. He, H. Jiang, J. Zhang, Y. Yin, Z. Jiang, J. C. Douglas, D.R. Dekel, M.D. Guiver, Self-crosslinked blend alkaline anion exchange membranes with Bi-continuous phase separated morphology to enhance ion conductivity, *J. Membr. Sci.* 597 (May 2019) (2020) 117769, <https://doi.org/10.1016/j.memsci.2019.117769>.
- [45] X. Gao, H. Yu, F. Xie, J. Hao, Z. Shao, High performance cross-linked anion exchange membrane based on the aryl-ether free polymer backbones for anion exchange membrane fuel cell application, *Sustain. Energy Fuels* 4 (2020) 4057–4066, <https://doi.org/10.1039/x0xx00000x>.
- [46] J. Xue, L. Liu, J. Liao, Y. Shen, N. Li, UV-crosslinking of polystyrene anion exchange membranes by azidated macromolecular crosslinker for alkaline fuel cells, *J. Membr. Sci.* 535 (January) (2017) 322–330, <https://doi.org/10.1016/j.memsci.2017.04.049>.
- [47] G.M. Carlomagno, G. Giorleo, Cross-Linked Polyethylene, vols. 577–588, 2006, <https://doi.org/10.1081/E-ECHP-120007720>.
- [48] J. Ponce-Gonzalez, D.K. Whelligan, L. Wang, R. Bance-Soualhi, Y. Wang, Y. Peng, H. Peng, D.C. Apperley, H.N. Sarode, T.P. Pandey, A.G. Divekar, S. Seifert, A. M. Herring, L. Zhuang, J.R. Varcoe, High performance aliphatic-heterocyclic benzyl-quaternary ammonium radiation-grafted anion-exchange membranes, *Energy Environ. Sci.* 9 (12) (2016) 3724–3735, <https://doi.org/10.1039/c6ee01958g>.
- [49] H.P. Brack, G.G. Scherer, Modification and characterization of thin polymer films for electrochemical applications, *Macromol. Symp.* 126 (1998) 25–49, <https://doi.org/10.1002/masy.19981260105>.
- [50] W.H. Lee, C. Crean, J.R. Varcoe, R. Bance-Soualhi, A Raman spectro-microscopic investigation of ETFE-based radiation-grafted anion-exchange membranes, *RSC Adv.* 7 (75) (2017) 47726–47737, <https://doi.org/10.1039/c7ra09650j>.
- [51] L. Gubler, S.A. Gürsel, G.G. Scherer, Radiation grafted membranes for polymer electrolyte fuel cells, *Fuel Cell.* 5 (3) (2005) 317–335, <https://doi.org/10.1002/fuce.200400078>.
- [52] D.W. Shin, M.D. Guiver, Y.M. Lee, Hydrocarbon-based polymer electrolyte membranes: importance of morphology on ion transport and membrane stability, *Chem. Rev.* 117 (6) (2017) 4759–4805, <https://doi.org/10.1021/acs.chemrev.6b00586>.
- [53] G.R. Strobl, M. Schneider, Direct evaluation of the electron density correlation function of partially crystalline polymers, *J. Polym. Sci. 2 Polym. Phys.* 18 (6) (1980) 1343–1359, <https://doi.org/10.1002/pol.1980.180180614>.
- [54] J.H. Choi, Y. Ye, Y.A. Elabd, K.I. Winey, Network structure and strong microphase separation for high ion conductivity in polymerized ionic liquid block copolymers, *Macromolecules* 46 (13) (2013) 5290–5300, <https://doi.org/10.1021/ma400562a>.
- [55] P. Cotanda, G. Sudre, M.A. Modestino, X.C. Chen, N.P. Balsara, High anion conductivity and low water uptake of phosphonium containing diblock copolymer membranes, *Macromolecules* 47 (21) (2014) 7540–7547, <https://doi.org/10.1021/ma501744w>.
- [56] Q.Q. Zhang, Q.Q. Zhang, J. Wang, S. Zhang, S. Li, Synthesis and alkaline stability of novel cardo poly(aryl ether Sulfone)s with pendent quaternary ammonium aliphatic side chains for anion exchange membranes, *Polymer* 51 (23) (2010) 5407–5416, <https://doi.org/10.1016/j.polymer.2010.09.049>.
- [57] R. Epszstein, E. Shaulsky, M. Qin, M. Elimelech, Activation behavior for ion permeation in ion-exchange membranes: role of ion dehydration in selective transport, *J. Membr. Sci.* 580 (January) (2019) 316–326, <https://doi.org/10.1016/j.memsci.2019.02.009>.
- [58] X. Li, Y. Yu, Q. Liu, Y. Meng, Synthesis and properties of anion conductive ionomers containing tetraphenyl methane moieties, *ACS Appl. Mater. Interfaces* 4 (7) (2012) 3627–3635, <https://doi.org/10.1021/am3007005>.
- [59] N. Ziv, W.E. Mustain, D.R. Dekel, The effect of ambient carbon dioxide on anion-exchange membrane fuel cells, *ChemSusChem* 11 (7) (2018) 1136–1150, <https://doi.org/10.1002/cssc.201702330>.
- [60] M. Mamlouk, K. Scott, Effect of anion functional groups on the conductivity and performance of anion exchange polymer membrane fuel cells, *J. Power Sources* 211 (2012) 140–146, <https://doi.org/10.1016/j.jpowsour.2012.03.100>.
- [61] T.P. Pandey, A.M. Maes, H.N. Sarode, B.D. Peters, S. Lavina, K. Vezzù, Y. Yang, S. D. Poynton, J.R. Varcoe, S. Seifert, M.W. Liberatore, V. Di Noto, A.M. Herring, Interplay between water uptake, ion interactions, and conductivity in an e-beam grafted poly(ethylene-Co-tetrafluoroethylene) anion exchange membrane, *Phys. Chem. Chem. Phys.* 17 (6) (2015) 4367–4378, <https://doi.org/10.1039/c4cp05755d>.
- [62] K.N. Grew, W.K.S. Chiu, A dusty fluid model for predicting hydroxyl anion conductivity in alkaline anion exchange membranes, *J. Electrochem. Soc.* 157 (3) (2010) B327, <https://doi.org/10.1149/1.3273200>.
- [63] V. Dubej, A. Maiti, S. Daschakraborty, Predicting the solvation structure and vehicular diffusion of hydroxide ion in an anion exchange membrane using nonreactive molecular Dynamics simulation, *Chem. Phys. Lett.* 755 (July) (2020) 137802, <https://doi.org/10.1016/j.cplett.2020.137802>.
- [64] D. Dong, W. Zhang, A.C.T. Van Duin, D. Bedrov, Grothuss versus vehicular transport of hydroxide in anion-exchange membranes: insight from combined reactive and nonreactive molecular simulations, *J. Phys. Chem. Lett.* 9 (4) (2018) 825–829, <https://doi.org/10.1021/acs.jpcclett.8b00004>.
- [65] C. Chen, Y.L.S. Tse, G.E. Lindberg, C. Knight, G.A. Voth, Hydroxide solvation and transport in anion exchange membranes, *J. Am. Chem. Soc.* 138 (3) (2016) 991–1000, <https://doi.org/10.1021/jacs.5b11951>.
- [66] W.E. Mustain, Understanding how high-performance anion exchange membrane fuel cells were achieved: component, interfacial, and cell-level factors, *Curr. Opin. Electrochem.* 12 (2018) 233–239, <https://doi.org/10.1016/j.coelec.2018.11.010>.
- [67] S. Gottesfeld, D.R. Dekel, M. Page, C. Bae, Y. Yan, P. Zelenay, Y.S. Kim, Anion exchange membrane fuel cells: current status and remaining challenges, *J. Power Sources* 375 (2018) 170–184, <https://doi.org/10.1016/j.jpowsour.2017.08.010>.
- [68] C.E. Diesendruck, D.R. Dekel, Water – a key parameter in the stability of anion exchange membrane fuel cells, *Curr. Opin. Electrochem.* 9 (2018) 173–178, <https://doi.org/10.1016/j.coelec.2018.03.019>.
- [69] T.J. Omasta, L. Wang, X. Peng, C.A. Lewis, J.R. Varcoe, W.E. Mustain, Importance of balancing membrane and electrode water in anion exchange membrane fuel cells, *J. Power Sources* 375 (2018) 205–213, <https://doi.org/10.1016/j.jpowsour.2017.05.006>.
- [70] W.E. Mustain, M. Chatenet, M. Page, Y.S. Kim, Durability challenges of anion exchange membrane fuel cells, *Energy Environ. Sci.* 13 (9) (2020) 2805–2838, <https://doi.org/10.1039/d0ee01133a>.